Available online at www.sciencedirect.com
SCIENCE DIRECT®
Journal of Solid State Chemistry 178 (2005) 2282–2291
JOURNAL OF SOLID STATE CHEMISTRY
www.elsevier.com/locate/jssc

Temperature and pressure dependent structural studies of the ordered double perovskites $Sr_2TbRu_{1-x}Ir_xO_6$

Qingdi Zhou[a], Brendan J. Kennedy[a,*], Kia S. Wallwork[b], Margaret M. Elcombe[b], Yongjae Lee[c], Thomas Vogt[c]

[a]*The School of Chemistry, The University of Sydney, Sydney, NSW 2006, Australia*
[b]*Bragg Institute, ANSTO, PMB 1, Menai, NSW 2234, Australia*
[c]*Physics Department, Brookhaven National Laboratory, Upton, NY 11973-5000, USA*

Received 21 February 2005; accepted 6 April 2005
Available online 9 June 2005

Abstract

High resolution powder diffraction studies are reported for the series of mixed RuIr perovskites $Sr_2TbRu_{1-x}Ir_xO_6$. Using a combination of synchrotron X-ray and neutron powder diffraction precise structures are established for the two end-member oxides, where the Tb oxidation state changes from +3 in the Ru oxide to +4 in the Ir containing oxide. The structures of both oxides are monoclinic. Composition dependent studies show that this valence transition is first order. Variable temperature diffraction show no evidence for any structural or valence state transitions. However, upon application of pressure $Sr_2TbRu_{0.3}Ir_{0.7}O_6$ undergoes a valence state transition at low pressures.

Keywords: Perovskite; Valence state; Crystal structure; Phase transition

1. Introduction

Oxides of the double perovskite family $A_2BB'O_6$ (where A is an alkaline earth cation and B and B' are transition metals or lanthanides) are of considerable interest as a consequence of their remarkable magnetic and electrical properties [1–3]. There is ample evidence that partial replacement of one of the B-site cations can have a dramatic effect on the observed magnetic and electrical properties, e.g., colossal magnetoresistance and superconductivity, especially when the B-site cation is a transition metal [4–8]. Altering the number of metal-ion d-electrons, and the energy of the d-levels relative to the oxygen $2p$ levels, can have significant impact on the electronic properties of transition metal oxides [9]. Small chemical substitutions can lead to a distortion of the structures of the double perovskites that are correlated with their electronic properties.

The series $Ba_2PrRu_{1-x}Ir_xO_6$ is an example in point. Magnetic measurements have shown that the pure Ru compound contains pentavalent Ru, whereas the pure Ir compound contains tetravalent Ir, thereby forming the two oxides $Ba_2Pr^{3+}Ru^{5+}O_6$ and $Ba_2Pr^{4+}Ir^{4+}O_6$ [10]. Solid solutions of the type $Ba_2PrRu_{1-x}Ir_xO_6$ can be prepared and detailed structural and magnetic studies show these oxides undergo a first-order valence state transition [10], accompanied by a monoclinic to tetragonal structural phase transition [11]. The valence state and structural transition can be induced by changes in either temperature [10,11] or pressure [12], with high pressure or low temperatures favoring the lower valence Pr^{4+}-containing tetragonal structures.

Recently, Doi and co-workers [13] reported a similar dependence of the valence state on the composition in the solid solutions $Sr_2TbRu_{1-x}Ir_xO_6$, although they did not consider the possibility that the valence state

*Corresponding author. Tel.: +61 2 9351 2742; fax: +61 2 9351 3329.
E-mail address: kennedyb@chem.usyd.edu.au (B.J. Kennedy).

0022-4596/$ - see front matter © 2005 Elsevier Inc. All rights reserved.
doi:10.1016/j.jssc.2005.04.030

transition was accompanied by a structural phase transition. Their published monoclinic lattice parameters for Sr_2TbIrO_6, obtained using powder X-ray diffraction measurements, are close to being metrically cubic $a' = a/\sqrt{2} = 4.067 \approx b' = b/\sqrt{2} = 4.073 \approx c' = c/2 = 4.069$ Å and the possibility that this has a higher symmetry structure cannot be discounted. Importantly, they did not consider the influence of temperature and/or pressure on the structures and valence states of the oxides.

Given the complex temperature and pressure dependence of the structure of the analogous $Ba_2PrRu_{1-x}Ir_xO_6$ series [10–12], coupled with the paucity of well characterized valence state transitions in transition metal oxides [14,15], we have re-investigated the structures of the series $Sr_2TbRu_{1-x}Ir_xO_6$ using high-resolution powder diffraction. We find that the application of moderate pressures can induce a valence state transition but surprisingly find no evidence for any temperature induced structural phase transitions.

2. Experimental

Polycrystalline samples of 10 members in the series of solid solutions $Sr_2TbRu_{1-x}Ir_xO_6$ were prepared by the reaction of the appropriate stoichiometric mixture of $SrCO_3$, Tb_4O_7, Ru and Ir. The reactants were intimately mixed in an agate mortar under acetone, placed in an alumina crucible and heated at temperatures of up to 1200 °C for 3 days with intermediate grindings.

The sample purity was established by powder X-ray diffraction measurements using Cu$K\alpha$ radiation on a Shimadzu D-6000 Diffractometer. Synchrotron X-ray powder diffraction patterns were collected on the high resolution Debye-Scherrer diffractometer at beamline 20B, the Australian National Beamline Facility, at the Photon Factory, Japan [16]. The samples were finely ground and loaded into 0.3-mm glass capillaries that were rotated during the measurements. All measurements were performed under vacuum to minimize air scattering. Data were recorded using two Fuji image plates. Each image plate is 20×40 cm and covers 40° in 2θ. The data were collected at a wavelength of 0.80282 Å (calibrated with a NIST Si 640c standard) over the 2θ range of 5–85° with step size of 0.01°. High temperature measurements were recorded in the same manner using a custom built furnace.

Neutron powder diffraction data were collected at the HIFAR facility operated by the Australian Nuclear Science and Technology Organisation (ANSTO) using the High Resolution Powder Diffractometer at a wavelength of 1.4928 Å [17]. Each sample was held in an aluminum capped vanadium sample holder and was rotated throughout the measurements. The diffractometer is equipped with 24 ^{3}He detectors individually separated by 5°. The patterns were collected at room temperature over the 2θ range 0–150° with step size of 0.05°.

A modified Merrill–Bassett diamond-anvil cell was used for the X-ray studies in the pressure range 0.0–6.0 GPa. The powdered sample together with a few small ruby chips was loaded into a 200 μm hole in a steel gasket. A methanol–ethanol–water (16:3:1) mixture was used as the hydrostatic pressure-transmitting medium. The pressure was calibrated by measuring the shift of the R_1 fluorescence line of ruby before and after each run. The variable pressure X-ray diffraction data were collected using synchrotron radiation at the bending magnet beamline, X7A, of the National Synchrotron Light Source at Brookhaven National Laboratory [18]. A wavelength of 0.69385 Å was selected using a channel cut Ge 1 1 1 monochromator.

Structural parameters were refined by the Rietveld method using the program RIETICA [19]. A pseudo-Voigt function was used to model the peaks. The background in the synchrotron diffraction measurements was fitted by linear interpolation between regions where there were no Bragg peaks. A polynomial function was used to estimate the background in the neutron diffraction profiles.

3. Results and discussion

3.1. Crystal structures of Sr_2TbRuO_6 and Sr_2TbIrO_6

The neutron diffraction data for the end-member ($x = 0$) compound Sr_2TbRuO_6, is shown in Fig. 1, and agrees with the previously published structure [20,21]. It is worth noting that the neutron scattering lengths of Tb and Ru are approximately equal, (0.721 and 0.738 fm, respectively) and as such it was not possible to distinguish these in the neutron diffraction measurements. Nevertheless, the pattern contained a number of reflections that could be indexed to an R-point mode. Usually this is taken as evidence for cation ordering [22,23] however, it should be stressed that an R-point mode is also associated with out-of-phase tilting of the BO_6 octahedra in successive layers [24]. The observation of these reflections in the neutron diffraction data shows that cation ordering and/or out-of-phase tilting is present. These structural features cannot be distinguished by extinction rules. This problem does not exist for the synchrotron X-ray diffraction data (Fig. 2), since the contribution to the intensity of the R-point reflections from the octahedra tilting is much less than that from the difference in scattering power of Tb and Ru. Furthermore, both the neutron and X-ray diffraction pattern show some X-point reflections that arise from a coupling of the M-point modes (responsible for the in-phase octahedral tilting) and the

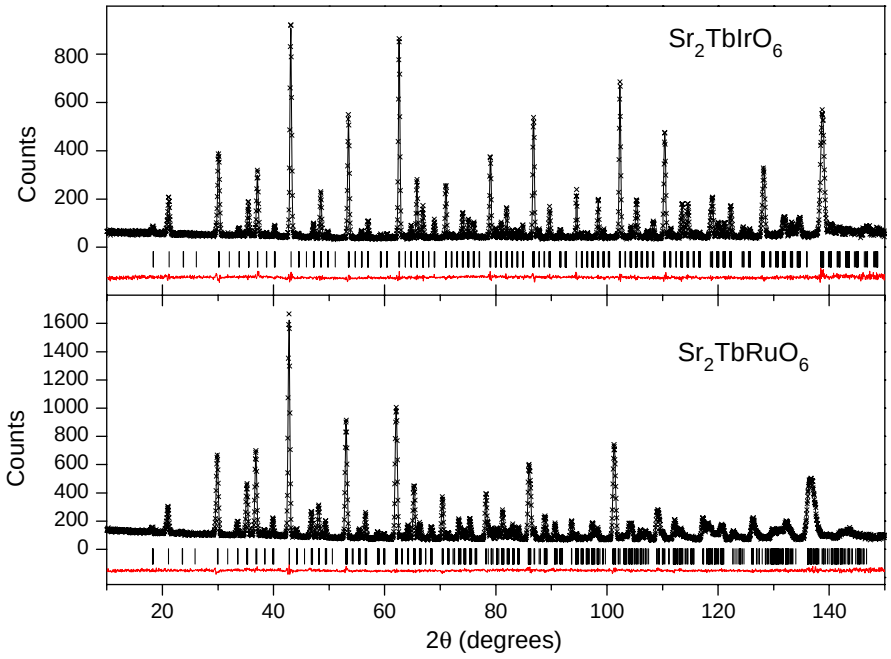

Fig. 1. Neutron diffraction profiles for Sr_2TbIrO_6 and Sr_2TbRuO_6 recorded at ambient temperature and pressure. The observed profile is indicated by the crosses and the calculated and difference profiles by the solid lines. The short vertical markers show the positions of the space group allowed Bragg reflections.

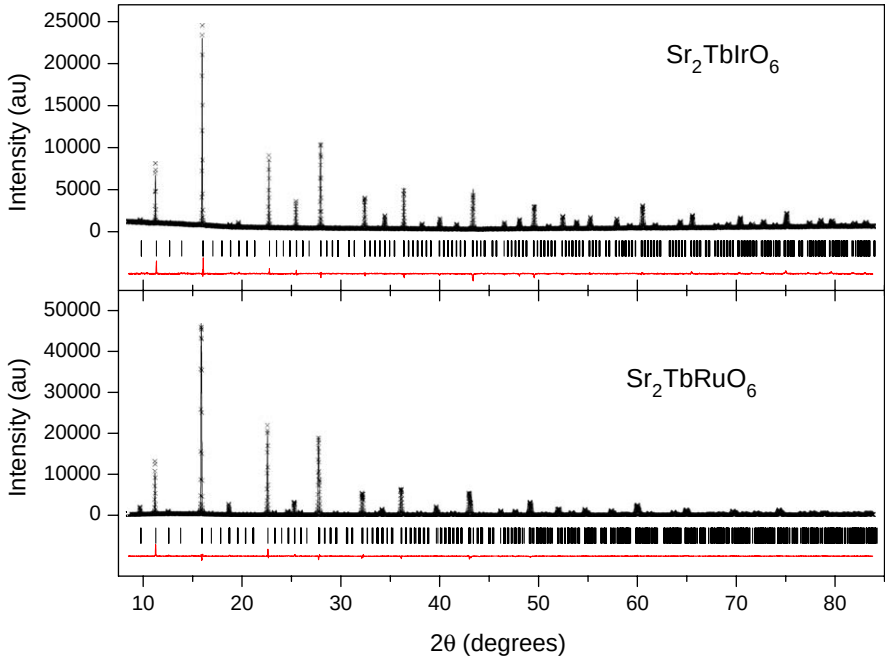

Fig. 2. Synchrotron X-ray diffraction profiles for Sr_2TbIrO_6 and Sr_2TbRuO_6 recorded at ambient temperature and pressure. The format of this figure is the same as Fig. 1.

R-point cation ordering. The most noticeable of these is the 1 1 1 reflection near $d = 3.66$ Å. The presence of such X-point reflections demonstrates that cation ordering along with M-point (+) and R-point (−) octahedral tilting is present. Thus the diffraction data shows that Sr_2TbRuO_6 is monoclinic with space group $P2_1/n$ where the Tb and Ru cations are ordered over two non-equivalent sites. The structural parameters refined using the neutron diffraction data are listed in Table 1 and selected bond distances and angles are listed in Table 2.

Table 1
Refined structural parameters for, monoclinic $P2_1/n$, Sr_2TbRuO_6 and Sr_2TbIrO_6 obtained using powder neutron diffraction data

Sr_2TbRuO_6				
$a = 5.7881(2)$ Å	90.244(2)°	$R_p = 3.59\%$		
$b = 5.8043(2)$ Å		$wR_p = 4.44\%$		
$c = 8.1917(3)$ Å		GOF = 1.54%		
Atom	x	y	z	B (Å^2)
Sr	0.9930(5)	0.4697(2)	0.7522(4)	0.41(3)
Tb	0	0	$\frac{1}{2}$	0.54(4)
Ru	0	0	0	0.06(3)
O1	0.4288(4)	0.5164(4)	0.7345(3)	0.68(3)
O2	0.3054(5)	0.7719(5)	0.4626(3)	0.66(4)
O3	0.2339(4)	0.2999(5)	0.4632(4)	0.76(5)
Sr_2TbIrO_6				
$a = 5.7558(2)$ Å	90.105(2)°	$R_p = 5.02\%$		
$b = 5.7494(2)$ Å		$wR_p = 6.28\%$		
$c = 8.1323(3)$ Å		GOF = 1.68%		
Atom	x	y	z	B (Å^2)
Sr	0.9952(8)	0.4759(4)	0.7507(10)	0.92(3)
Tb	0	0	$\frac{1}{2}$	0.59(5)
Ir	0	0	0	0.72(7)
O1	0.4349(9)	0.5094(6)	0.7442(7)	0.93(6)
O2	0.2877(8)	0.7747(11)	0.4699(7)	1.12(9)
O3	0.2263(9)	0.2851(11)	0.4707(7)	0.97(8)

The numbers in parentheses are estimated standard deviations of the last significant figure. Where no standard deviation is given, the parameter was not refined.

Table 2
Selected Bond distances and tilt angles obtained from refinements using neutron diffraction data

Bond	Sr_2TbRuO_6	Sr_2TbIrO_6
Tb–O(1) Å	2.214(3)	2.114(6)
Tb–O(2) Å	2.231(3)	2.117(4)
Tb–O(3) Å	2.227(3)	2.107(6)
Tb–O (avg)	2.224	2.113
θ°	12.9	10.0
φ°	8.4	6.7
B–O(1) Å	1.969(3)	2.022(5)
B–O(2) Å	1.962(3)	2.012(5)
B–O(3) Å	1.951(3)	2.016(6)
B–O (avg)	1.961	2.017
θ°	11.2	10.5
φ°	7.6	7.1

The tilt about the, cubic, four-fold (001) axis is given by φ and that about the two-fold (110) axis by θ.

A diagram of the structure is given in Fig. 3. The average Ru–O distance 1.961 Å is similar to that of other Ru^V oxides including Ba_2PrRuO_6 [12] and Sr_2YRuO_6 [25]. Likewise the average Tb–O distance 2.224 Å appears typical of a Tb^{III} oxide, and is similar to the distance of 2.283 Å seen in Sr_3TbRhO_6 [26].

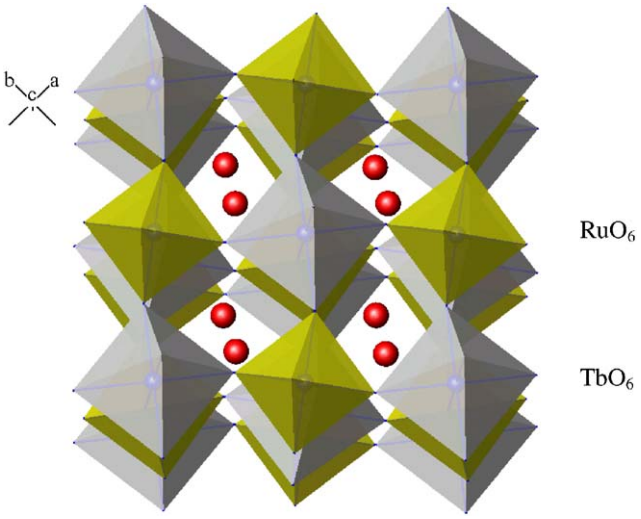

Fig. 3. Representation of the structure of Sr_2TbRuO_6. The spheres are the Sr atoms and the octahedra are the TbO_6 and RuO_6 units.

The powder neutron diffraction for the second end-member of the series ($x = 1$) Sr_2TbIrO_6 is striking in its apparent simplicity—all the peaks could be indexed on the basis of a primitive cubic cell with $a = 8.13$ Å (Fig. 1). In this case the scattering length of Tb and Ir are sufficiently different (0.738 and 1.060 for Tb and Ir, respectively) so that cation ordering and out-of-phase tilting are both expected to contribute to the intensity of the R-point reflections. The observation of the X-point reflections in the X-ray diffraction profile (Fig. 2) shows that a combination of cation ordering and in-phase and out-of-phase tilting of the octahedra are present. This cannot occur in a simple primitive cubic perovskite and we conclude that the most appropriate space group is the monoclinic $P2_1/n$. This space group has been suggested in previous studies of this material [27,28]. Despite the apparent simplicity of the neutron diffraction pattern the refinement in this monoclinic space group was, perhaps surprisingly, easy and yielded seemingly precise structural parameters. This is apparently a consequence of the observation, and use of, the well-resolved superlattice reflections in establishing both the cell parameters and atomic coordinates.

Just as the average refined Tb–O distance in Sr_2TbIrO_6, 2.113 Å, is noticeably shorter than the one found for Sr_2TbRuO_6, 2.224 Å, the average refined Ir–O distance, 2.017 Å, is noticeably longer than the one found in Ir(V) oxides such as Sr_2FeIrO_6, 1.97 Å [29] and Ln_2NaIrO_6 1.967 [30]. The average Tb–O distance, 2.113 Å is typical of other Tb(IV) oxides such as 2.15 Å in cubic $BaTbO_3$ [31] and 2.132 Å in $Ba_3TbRu_2O_9$ [32]. These distances establish the difference in the Tb oxidation state between the two end-members. The observed structures were compared with those predicted using the program SPUDS [33]. SPUDS predicts a more

distorted metric for Sr_2TbRuO_6 $a = 5.739$, $b = 5.927$, $c = 8.242$ Å, $\beta = 90.04^\circ$ than is actually observed in Table 1, suggesting that electronic and/or magnetic effects diminish the structural distortion. Likewise the observed volume for Sr_2TbRuO_6 (275.20 Å^3) is somewhat smaller than that estimated by SPUDS (280.37 Å^3), presumably for a similar reason.

The agreement between the observed and the SPUDS calculated structure is somewhat better for Sr_2TbIrO_6. Calculated $a = 5.700$, $b = 5.829$, $c = 8.148$ Å, $\beta = 90.01^\circ$ and observed $a = 5.7558$, $b = 5.7494$, $c = 8.1323$ Å, $\beta = 90.105^\circ$. These calculations show that the $P2_1/n$ structure is expected to be the most stable at room temperature, with simpler tilt systems such as $I4/m$ ($a^0a^0c^-$) unlikely to be observed except at very high temperatures. Two other possibilities $I2/m$ and $R\bar{3}$ are more stable than $I4/m$, but again both are less favorable than $P2_1/n$ and are unlikely to be observed.

The $P2_1/n$ monoclinic structure arises from the combination of cation ordering and tilting of the octahedra, the latter being described in the notation of Glazer [34] as $a^-a^-c^+$; i.e., out-of-phase tilting occurs about the $[110]_p$ pseudo-cubic axis and in-phase tilting occurs about the $[001]_p$-axes. In addition to providing an accurate measure of the various bond distances, the refined atomic co-ordinates were used to calculate the magnitude of the tilts about the 0 0 1 (φ) and 1 1 0 (θ) axes of the cubic aristotype as described by Groen [35]. We observe (Table 2) the magnitude of the tilt about the 0 0 1 axis to be smaller than that about the 1 1 0 axis. In both structures both these tilts are significantly greater than zero and any continuous transition to a higher symmetry structure therefore appears unlikely.

The stability of the double perovskites can be estimated using a modification of the Goldschmidt tolerance factor [36], $\phi = \sqrt{2}r_A/(r_B + r_O)$ where r_B is the weighted average of the ionic radii of the two B-site cations, and r_A and r_O the ionic radii of the A-site and oxygen ions, respectively. For $Sr_2Tb^{4+}Ir^{4+}O_6$ $\phi = 0.97$ and for $Sr_2Tb^{3+}Ru^{5+}O_6$ $\phi = 0.95$. Teraoka [37] has suggested that monoclinic structures in $P2_1/n$ will occur when $\phi < 0.90$. Increasing values of ϕ will favor higher symmetry structures. The structure of the Ir compound is less distorted, in terms of both the observed tilt angles and the monoclinic angle, than that of the Ru compound in keeping with the increase in the tolerance factor. For both structures the calculated value of ϕ is noticeably greater than 0.90 demonstrating that, like the original Goldschmidt tolerance factor, the size remains at best a crude estimator for the possible space group.

3.2. Room temperature crystal structures of $Sr_2TbRu_{1-x}Ir_xO_6$

Having established the symmetry of the two end-members to be monoclinic in $P2_1/n$ the structures of the remaining eight samples were then also refined using this space group. Fig. 4 shows the refined lattice parameters for the entire composition range. The samples can clearly be divided into two classes, those with $x < 0.8$ having a larger unit cell, similar to that observed for Sr_2TbRuO_6 and those with $x > 0.8$ that have a smaller unit cell reminiscent of Sr_2TbIrO_6. The sample with $x = 0.8$ contains a mixture of the two phases as shown in Fig. 5. The ratio of the two phases, obtained using the Rietveld analysis is estimated to be 59:41% in remarkable agreement with the previous work of Doi et al. [13].

Two features worth noting in Fig. 4 are, firstly, the clear difference in the value of the monoclinic angle β between the two series. The larger volume cells have a β

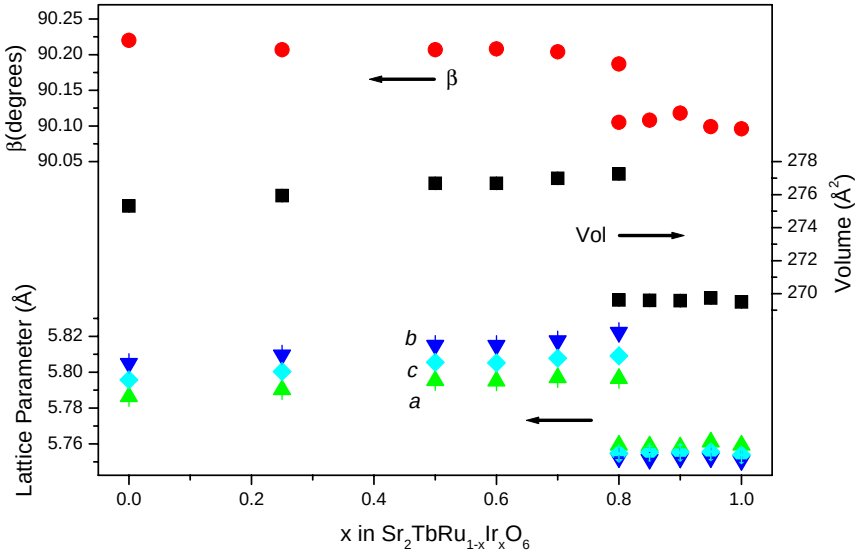

Fig. 4. Composition dependence of the cell parameters and volume in the series $Sr_2TbRu_{1-x}Ir_xO_6$. For clarity the c-parameter has been reduced by $\sqrt{2}$. Note the reversal of the a- and b-parameters at the phase transition.

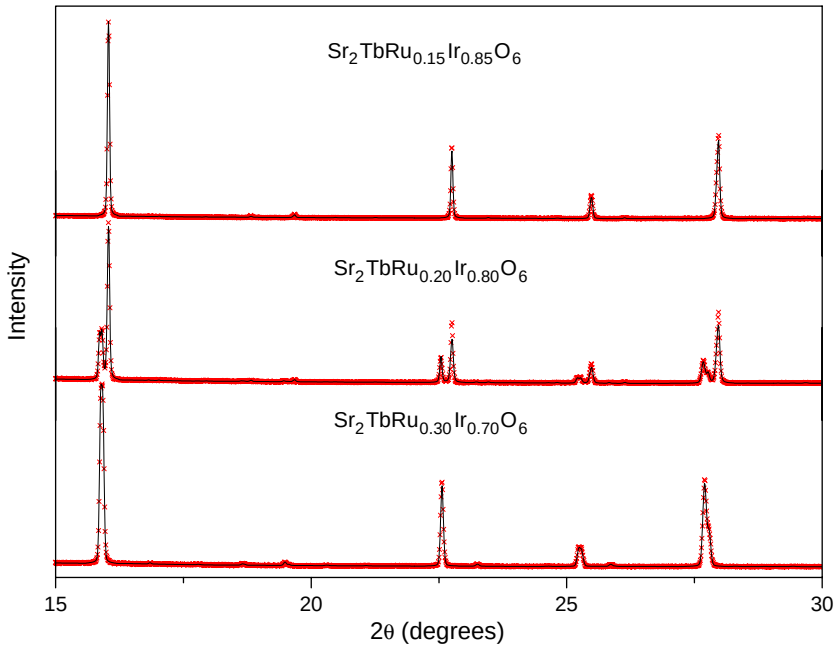

Fig. 5. Portions of the diffraction patterns for three samples with $x = 0.85$, 0.80 and 0.70 showing the co-existence of the two phases in the $x = 0.8$ sample. Note also the lack of any obvious broadening or splitting of the Bragg reflections in the pattern of $Sr_2TbRu_{0.15}Ir_{0.85}O_6$.

angle close to 90.2°, whereas the smaller Ir rich cells have a $\beta \approx 90.1°$. Secondly, the transition between the two monoclinic cells involves a reversal of the a/b ratio from less than 1 in the larger Ru rich cells to greater than 1 in the smaller Ir rich cells. These two features allow for the easy identification of the structural type.

Bond distances were estimated for each of the phases from the refined structural parameters, and as illustrated in Fig. 6 the transition between the two classes involves a large reduction in the average Tb–O distances and a smaller increase in the average Ru–O distance. These changes are consistent with a concurrent change from Tb^{3+} to Tb^{4+} and from Ru^{5+} to Ru^{4+} near $x = 0.8$.

The smaller size of the Ir rich oxides is a consequence of the rate of change of the two polyhedra. The relative decrease in ionic radii in going from Tb^{3+} to Tb^{4+} (0.16 Å) is much larger than the rate of increase for M^{5+} (M = Ru, Ir) to M^{4+} (0.055 Å) [38]. Therefore a valence state transition of the type $Ba_2Tb^{3+}M^{5+}O_6$ to $Ba_2Tb^{4+}M^{4+}O_6$ is expected to result in a contraction in the cell volume, since the volume of the TbO_6 octahedron should decrease much more rapidly than the increase in the volume of the MO_6 octahedron. Examination of the volumes of the TbO_6 and MO_6 octahedra [39] in the two end-members proves this to be the case. The volume for the TbO_6 octahedra decreasing from 13.6 $Å^3$ at $x = 1$ to 11.9 $Å^3$ at $x = 0$ whereas that of the MO_6 octahedra shows a very small increase over the same composition range, from 10.1 $Å^3$ in Sr_2TbRuO_6, to 10.9 $Å^3$ in Sr_2TbIrO_6.

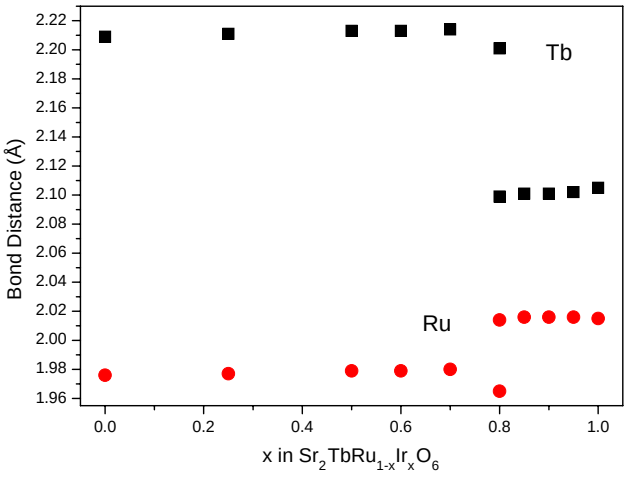

Fig. 6. Composition dependence of the average Ru–O and Tb–O bond distances in the series $Sr_2TbRu_{1-x}Ir_xO_6$.

We conclude that the two oxides Sr_2TbRuO_6 and Sr_2TbIrO_6 do not form a complete solid solution, rather there is a miscibility gap near $x = 0.8$. This is despite the structures remaining in the same monoclinic space group across the entire composition range.

3.3. Variable temperature structural studies

The relatively large difference in the volume of the two structural types suggested that it may be possible to induce a transition to the larger volume

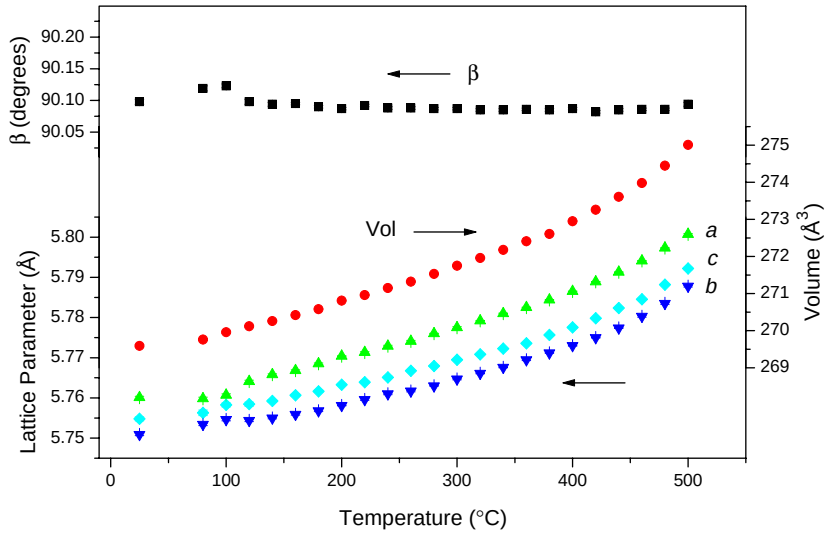

Fig. 7. Temperature dependence of the cell parameters and volume for $Sr_2TbRu_{0.1}Ir_{0.9}O_6$.

Tb^{3+}-containing configuration by heating a Tb^{4+}-containing, Ir rich compound. As noted above, the analysis of the structural features using SPUDS suggests that these oxides are unlikely to undergo any structural transitions involving only the loss of tilts at temperatures up to 800 °C. It is evident from Fig. 7, that heating $Sr_2TbRu_{0.1}Ir_{0.9}O_6$ to 500 °C results in a relatively smooth increase of the lattice parameters and cell volume. There is no obvious indication for a two-phase region, nor is there any suggestion of a discontinuity that may accompany a first-order phase transition. Possibly the best indication that no valence state transition has occurred is the consistency of the monoclinic angle (Fig. 7). The composition dependent studies show the Tb^{3+} oxides are more distorted and have $\beta \approx 90.2^\circ$ whereas the Tb^{4+} containing oxides have $\beta \approx 90.1^\circ$. The monoclinic angle in $Sr_2TbRu_{0.1}Ir_{0.9}O_6$ remains essentially constant over the entire temperature range. Likewise the average Tb–O and B–O bonds distances remain essentially constant upon heating to 500 °C and we conclude, therefore, that terbium remains trivalent in this oxide.

As noted above, the sample of $Sr_2TbRu_{0.2}Ir_{0.8}O_6$ studied is a mixture of two perovskite phases at room temperature. Heating this to 200 °C did not alter the appearance of the diffraction pattern. Quantification of the two phases suggests there is, at most, a very small decrease in the amount of the smaller Tb^{4+} containing structure from 59.0(3)% to 56.0(3)%.

The possibility that the Tb^{3+} containing oxides may undergo a structural transition was also investigated by heating a sample of $Sr_2TbRu_{0.4}Ir_{0.6}O_6$ to 500 °C. This resulted in a progressive increase in the cell parameters, comparable to that of the $Sr_2TbRu_{0.1}Ir_{0.9}O_6$ material. Reflections indicative of the X-point and M-point modes persisted to the highest temperature showing by in-phase and out-of-phase tilting of the BO_6 octahedra persisted and that no structural phase transition had occurred.

3.4. Variable pressure structural studies

An alternative to temperature for controlling the volume of a structure is pressure. The application of high pressure favors more dense, lower volume, cells. X-ray diffraction patterns were collected as a function of pressure for four samples with $x = 0$, 0.25, 0.5 and 0.70. The data collected on samples contained within the diamond anvil cell are of lower quality due to their limited q-range than those obtained for samples contained in a capillary. Whilst it was possible to obtain accurate lattice parameters, and hence cell volumes from these data, they were not suitable for structural refinements, rather lattice parameters were estimated using the Le Bail method as implemented in the program RIETICA [19].

Diffraction data were collected at pressures of up to 7.3 GPa for $Sr_2TbRu_{0.3}Ir_{0.7}O_6$, this composition being adjacent to the observed transition. At all pressures the patterns were well fitted (using a Le Bail approach) to a single monoclinic structure. Even at 0.8 GPa, the lowest pressure achieved for this composition, the cell volume was noticeably smaller than that obtained under ambient conditions 268.2(2) vs. 276.99(2) and the a/b ratio was less than 1. A linear fit to the observed cell volumes yielded a value of ≈ 269 Å^3 at zero applied pressure. These results suggest a transition to the lower volume Tb^{4+} containing state had occurred. Progressively increasing the pressure to 7.3 GPa results in a nearly linear reduction in the cell volume with the pattern broadening slightly at the highest pressure suggesting non-ideal hydrostatic conditions.

The bulk modulus, B_0, of $Sr_2TbRu_{0.3}Ir_{0.7}O_6$ was calculated to be 196(10) GPa, and was obtained by fitting a second-order Birch–Murnaghan [40] equation of state to the pressure dependence of the volume of the monoclinic phase. This is comparable to that found for a simple perovskite-type such as $LaAlO_3$ [41] and $PrAlO_3$ [42] which have values of 190(5) and 205(8) Gpa, respectively. These values are noticeably higher than observed in $Ba_2PrRu_{0.8}Ir_{0.2}O_6$, 139(10) GPa [12] and $LaCoO_3$, 150(2) GPa [43] both of which display pressure induced transitions.

In an attempt to observe evidence for the co-existence of the two phases we next examined the pressure dependence of the structure of $Sr_2TbRu_{0.5}Ir_{0.5}O_6$ in the expectation that this may transform to the lower volume state at a higher pressure than is observed for $Sr_2TbRu_{0.3}Ir_{0.7}O_3$. The pattern recorded at 0.4 GPa was well fitted to a single phase model with a volume of 276.3 $Å^3$, which is in good agreement with the volume found from data collected on a capillary sample. Application of moderate pressure ~2 GPa resulted in a dramatic broadening of the diffraction peaks and a remarkable reduction in the volume to ~271.9 $Å^3$. Increasing the pressure further resulted in an essentially linear reduction in the cell volume without further increase in the peak widths, in fact the peaks narrowed slightly as the pressure was increased to 6.7 GPa. The pressure dependence of the peak widths does not appear to be symptomatic of non-hydrostatic conditions as the luminescence signal from the ruby stayed sharp. As evident from Fig. 8, the cell volume at the highest pressure attained is very similar to that observed for $Sr_2TbRu_{0.3}Ir_{0.7}O_6$ at high pressures and we propose that this represents the Tb^{IV} configuration.

Although the pattern for $Sr_2TbRu_{0.5}Ir_{0.5}O_6$ recorded at 2 GPa could be fitted to a single phase model, albeit with larger than expected peak widths, it could also be fitted to a two phase model with cell volumes of 273.6(1) and 262.4(2) $Å^3$. The co-existence of the two phases is evidence of a first-order phase transition. The patterns recorded at intermediate pressures, 3.0 and 4.7 GPa could be fitted to either a single-phase or a two-phase model and it was not possible to distinguish between these as a consequence of the broadness of the peaks. The use of the two phase models did not result in a unique solution thus the pressure–volume behavior reported in Fig. 8 is that for a single-phase model.

We have also examined the structures of the end-member $x = 0$ compound Sr_2TbRuO_6 and find no evidence for any transition below 5.14 GPa. The bulk modulus, B_0, of this material, obtained by fitting a second-order Birch–Murnaghan [40] equation of state, was calculated to be 142(8) GPa. This is similar to the value observed in $Ba_2PrRu_{0.8}Ir_{0.2}O_6$ [12]. Above 5 GPa the diffraction pattern becomes more complicated suggesting the material may undergo another phase transition. The structure of this high pressure phase has not yet been established.

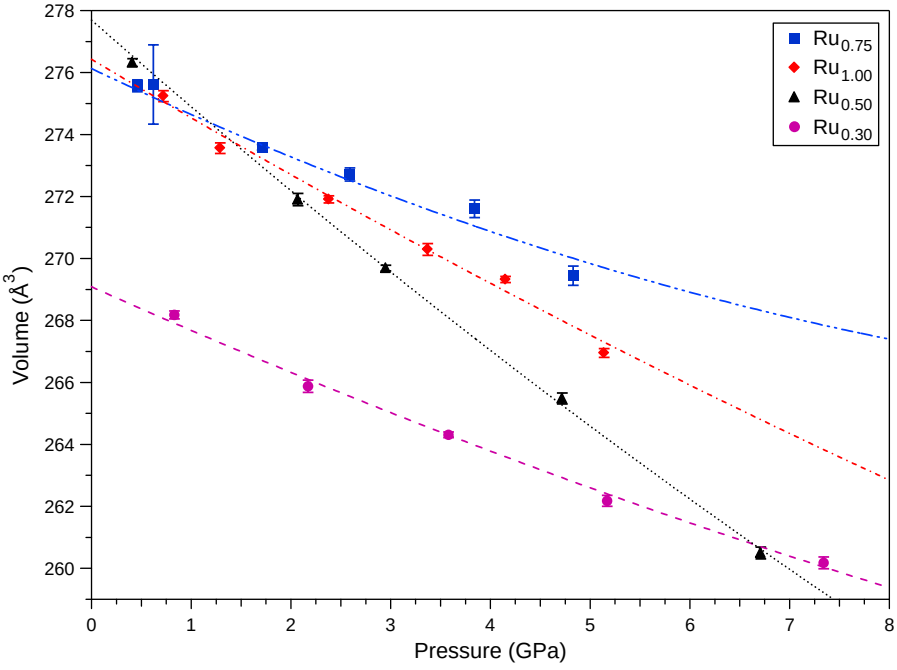

Fig. 8. Pressure-dependence of the cell volumes for the series of double perovskites $Sr_2TbRu_{1-x}Ir_xO_6$. The Birch–Murnaghan, second-order fits to the observed data are also shown. Where not apparent the errors in volume are smaller than the symbols.

3.5. Further discussion and concluding remarks

We are now confronted by an interesting dilemma as to why a temperature induced valence transition is not observed in any members of the series $Sr_2TbRu_{1-x}Ir_xO_6$ whereas a facile transition is observed in the closely related $Ba_2PrRu_{1-x}Ir_xO_6$ series. A major difference between the two systems is that the valence state transition in the Pr oxides is associated with a structural phase transition whereas the structures of the two end member Tb oxides are isostructural. Other than the difference in the lanthanide cation, the largest difference between the two systems is the magnitude of the structural distortion arising from the change in the *A*-site cation. The tilting of the octahedra in perovskite oxides is a consequence of the less than optimal size of the *A*-site cation. In Ba_2PrRuO_6 the magnitude of the octahedral tilting is considerably less than that observed in Sr_2TbRuO_6. In Ba_2PrIrO_6 one of the tilts becomes zero, whereas the same tilt remains much larger than zero in Sr_2TbIrO_6. It is possible that the larger distortion observed in the Sr compounds acts as an energy barrier for the valence state transition. The importance of the structural distortion in driving the valence states in these oxides is further illustrated by the observation that Ba_2TbIrO_6, the structure of which should be less distorted than that of Sr_2TbIrO_6, contains Tb^{3+}. Efforts are underway to confirm that the valence of the two *B*-site cations in these types of double perovskites can be tuned by control of the octahedral tilting through variation of the *A*-site cation.

We note that temperature and pressure are complementary in the study of phase transitions, however, they do not always cause the same effect. This is evident for $CaFeO_3$ [44,45] where cooling the sample results in a first-order charge disproportion transition to the same monoclinic structure as observed here, but high pressure measurements result in a high-spin to low-spin transition.

Acknowledgments

BJK thanks the Australian Research Council for support for his work on perovskites. The work performed at the Australian National Beamline Facility was supported by the Australian Synchrotron Research Program, which is funded by the Commonwealth of Australia under the Major National Research Facilities program. The Australian Institute of Nuclear Science and Engineering supported the neutron diffraction experiments. Work at Brookhaven is supported by the US Department of Energy, Division of Materials Sciences under contract No. DE-AC02-98CH10886. The assistance of Dr. James Hester at the ANBF is gratefully acknowledged.

References

[1] K.L. Kobayashi, T. Kimura, H. Sawada, K. Terakura, Y. Tokura, Nature 395 (1998) 677.
[2] S. Jin, T.H. Tiefel, M. McCormack, R.A. Fastnacht, R. Ramesh, L.H. Chen, Science 264 (1994) 413.
[3] A. Moreira dos Santos, A.K. Cheetham, T. Atou, Y. Syono, Y. Yamaguchi, K. Ohoyama, H. Chiba, C.N.R. Rao, Phys. Rev. B 66 (2002) 064425.
[4] M.K. Wu, D.Y. Chen, F.Z. Chien, S.R. Sheen, D.C. Ling, C.Y. Tai, G.Y. Tseng, D.H. Chen, F.C. Zhang, Z. Phys. B: Condens. Matter 102 (1997) 37.
[5] E. Granado, Q. Huang, J.W. Lynn, J. Gopalakrishnan, K. Ramesha, Phys. Rev. B 70 (2004) 214,416.
[6] A.V. Samoilov, G. Beach, C.C. Fu, N.C. Yeh, R.P. Vasquez, Phys. Rev. B 57 (1998) R14032.
[7] M.A. Subramanian, A.W. Sleight, Solid State Sci. 4 (2002) 347.
[8] Y. Doi, Y. Hinatsu, K. Oikawa, Y. Shimojo, Y. Morii, J. Alloys Compds. 323 (2001) 455.
[9] P.A. Cox, Transition Metal Oxides: An Introduction to their Electronic Structure and Properties, Clarendon Press, Oxford, 1992.
[10] M. Wakeshima, Y. Izumiyama, Y. Doi, Y. Hinatsu, Solid State Commun. 120 (2001) 273.
[11] L. Li, B.J. Kennedy, J. Solid State Chem. 177 (2004) 3290.
[12] B.J. Kennedy, L. Li, Y. Lee, T. Vogt, J. Phys.: Condens. Matter 16 (2004) 3295.
[13] Y. Doi, Y. Hinatsu, K. Oikawa K, Y. Shimojo, Y. Morii, J. Mater. Chem. 10 (2000) 1731.
[14] P.M. Woodward, D.E. Cox, E. Moshopoulou, A.W. Sleight, S. Morimoto, Phys. Rev. B 62 (2000) 844.
[15] A. Jayaraman, G.A. Kourouklis, L.G. Van Uitert, Phys. Rev. B 36 (1987) 8547.
[16] T.M. Sabine, B.J. Kennedy, R.F. Garrett, G.J. Foran, D.J. Cookson, J. Appl. Crystallogr. 28 (1995) 513.
[17] C.J. Howard, C.J. Ball, R.L. Davis, M.M. Elcombe, Aust. J. Phys. 36 (1983) 507.
[18] T. Vogt, G. Schneider, J.A. Hriljac, G. Yang, J.S. Abell, Phys. Rev. B 63 (2001) 220505.
[19] C.J. Howard, B.A. Hunter, A Computer Program for Rietveld Analysis of X-ray and Neutron Powder Diffraction Patterns, Lucas Heights Research Laboratories, NSW, Australia, 1998, pp. 1–27.
[20] N.G. Parkinson, P.D. Hatton, J.A.K. Howard, C. Ritter, R.M. Ibberson, M.K. Wu, J. Phys.: Condens. Matter 16 (2004) 7611.
[21] Y. Izumiyama, Y. Doi, M. Wakeshima, Y. Hinatsu, Y. Shimojo, Y. Morii, J. Phys.: Condens. Matter 13 (2001) 1303.
[22] R.H. Mitchell, Perovskites: Modern and Ancient, Almaz Press, Ontario, Canada, 2002.
[23] M.T. Anderson, K.B. Greenwood, G.A. Taylor, K.R. Poeppelmeir, Prog. Solid State Chem. 22 (1993) 197.
[24] C.J. Howard, B.J. Kennedy, P.M. Woodward, Acta Crystallogr. B 59 (2003) 463.
[25] P.D. Battle, W.J. Macklin, J. Solid State Chem. 52 (1984) 138.
[26] R.C. Layland, S.L. Kirkland, H.C. zur Loye, J. Solid State Chem. 139 (1998) 79.
[27] D. Harada, M. Wakeshima, Y. Hinatsu, J. Solid State Chem. 145 (1999) 256.
[28] D. Harada, M. Wakeshima, Y. Hinatsu, K. Ohoyama, Y. Yamaguchi, J. Phys.: Condens. Matter 12 (2000) 3229.
[29] P.D. Battle, C.P. Grey, M. Hervieu, C. Martin, C.A. Moore, Y. Paik, J. Solid State Chem. 175 (2003) 20.
[30] M.J. Davis, S.J. Mugavero, K.I. Glab, M.D. Smith, H.C. zur Loye, Solid State Sci. 6 (2004) 413.
[31] W.T. Fu, D. Visser, K.S. Knight, D.J.W. Ijdo, J. Solid State Chem. 177 (2004) 1667.

[32] Y. Doi, M. Wakeshima, Y. Hinatsu, A. Tobo, K. Ohoyama, Y. Yamaguchi, J. Alloys Compds. 344 (2002) 166.
[33] M. Lufaso, P.M. Woodward, Acta Crystallogr. B 57 (2001) 725.
[34] A.M. Glazer, Acta Crystallogr. B 28 (1972) 3384.
[35] W.A. Groen, F.P.F. Van Berkel, D.J.W. Ijdo, Acta Crystallogr. C 42 (1986) 1472.
[36] V.M. Goldschmidt, Skrifter Norsk. Vidensk. Akad. Klass. 8 (1) (1926) 2.
[37] Y. Teraoka, M.D. Wei, S. Kagawa, J. Mater. Chem. 8 (1998) 2323.
[38] R.D. Shannon, Acta Crystallogr. A. 32 (1976) 751.
[39] T. Balic-Zunic, I. Vikovic, J. Appl. Crystallogr. 29 (1996) 305.
[40] F. Birch, Phys. Rev. 71 (1947) 809.
[41] B.J. Kennedy, T. Vogt, C.D. Martin, J.B. Parise, J.A. Hriljac, Chem. Mater. 14 (2002) 2664.
[42] B.J. Kennedy, T. Vogt, C.D. Martin, J.B. Parise, J.A. Hriljac, J. Phys.: Condens. Matter 13 (2001) L925.
[43] T. Vogt, J.A. Hriljac, N.C. Hyatt, P.M. Woodward, Phys. Rev. B 67 (2003) 140,401.
[44] T. Kawakami, S. Nasu, T. Sasaki, K. Kuzushita, S. Morimoto, S. Endo, S. Kawasaki, M. Takano, J. Phys.: Condens. Matter 14 (2002) 10,713.
[45] T. Takeda, R. Kanno, Y. Kawamoto, M. Takano, S. Kawasaki, T. Kamiyama, F. Izumi, Solid State Sci. 2 (2000) 673.